Cite This: J. Nat. Prod. XXXX, XXX, XXX-XXX

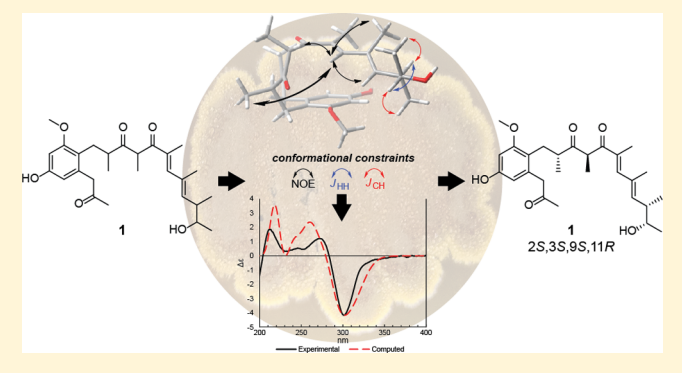
Polyketides from Marine-Derived *Aspergillus porosus*: Challenges and Opportunities for Determining Absolute Configuration

George F. Neuhaus, Donovon A. Adpressa, Torsten Bruhn, and Sandra Loesgen*, So

Supporting Information

Downloaded via UNIV OF FLORIDA on September 26, 2019 at 20:11:29 (UTC). See https://pubs.acs.org/sharingguidelines for options on how to legitimately share published articles.

ABSTRACT: Fungal natural products have inspired and enabled countless modern therapeutics. During a survey of the secondary metabolites of endophytic fungi, we found that Aspergillus porosus produces new polyketides with interesting structural features named porosuphenols A–D (1, 2, 3a, and 3b). The structural elucidation of these metabolites was performed with 1D and 2D NMR techniques, Mosher ester analysis, J-based conformational analysis, and isotope exchange studies. The absolute configuration of these compounds was determined using typical approaches including comparative analysis of experimental NMR and electronic circular dichroism spectra with DFT calculations. However, these efforts did not provide conclusive results for



porosuphenol A (1). To resolve this issue, we applied a strategy in which NMR data guide the conformer search. Herein are presented the structure elucidation of porosuphenols A-D as a case study in the challenges and opportunities for determination of absolute configuration. Lastly, bioassay-guided fractionation of cytotoxic fractions resulted in the additional isolation of pimarane diterpenes, sphaeropsidin A (4), and aspergiloid E (5).

etermining the absolute configuration of a molecule is a vital step in reaching a complete understanding of its structure. Even today, with state-of-the-art spectroscopic techniques at our disposal, the continued challenge of this problem is evident by the number of recent revisions to natural product configurational assignments. Natural products in particular, which inspire the majority of clinically approved drugs,² often pose difficult obstacles in the determination of absolute configuration due to their numerous asymmetric centers and overall complex chemical structures. This challenge is amplified when working with structures that have substantial conformational freedom. Molecular flexibility can be an obstacle in structure elucidation based on solution NMR experiments, as the experimentally observed parameters are averages of multiple conformations on the NMR time scale. Similarly, computational models provide predictions for spectroscopic parameters that can be invaluable for configurational assignment, but models must be developed using correctly identified conformers.3 Modeling the full conformational space and solvation effects of flexible structures can be prohibitively expensive computationally and may even require more accuracy than current methods can provide. Nonetheless, determining the absolute configuration of natural products is imperative for understanding their biological activity and also for developing drug leads. Herein, we report on four new linear polyketides, porosuphenols A, B, C, and D (1, 2, 3a, and 3b), as well as two known metabolites (4 and 5) from Aspergillus

porosus. Initial efforts to identify the absolute configuration of porosuphenol A (1) were obstructed by the conformational flexibility of the structure and inconclusive modeling results. As an alternative approach to the usually applied Boltzmann weighting, we employed experimentally informed conformational restrictions that were developed for the structure determination using NMR calculations (CASE-3D).^{3a}

As part of an ongoing research program to explore the chemical diversity of endophytic fungi, we performed chemical- and bioactivity-guided screening of extracts from a marine-derived endophyte, A. porosus. ⁴ The organic extract of a malt-based broth culture was found to contain a class of new polyketides (1-3), exhibiting a dynamic diene-dione functionality within a flexible carbon chain. The closest structural relative of these new fungal polyketides can be found in a benzaldehyde intermediate within the azaphilone biosynthetic pathway.⁵ The common benzenediol is functionalized with a highly methylated⁶ polypropionate-like⁷ side chain and a methyl ketone, both containing a fully reduced carbon attached directly to the aromatic ring. This is unlike the common fungal benzenediol lactones⁸ and azaphilones,⁹ in which carbonyl groups are directly attached to the aromatic ring. Other structurally related compounds are the acyclic tetraprenylqui-

Received: May 3, 2019



[†]Department of Chemistry, Oregon State University, Corvallis, Oregon 97331, United States

[‡]Bundesinstitut für Risikobewertung, Berlin 12277, Germany

Chart 1

nols found in brown algae, ¹⁰ in which the benzenediol core is prenylated to create the acyclic side chain.

Alongside the structurally interesting porosuphenol polyketides, two known diterpene cytotoxins, sphaeropsidin A and aspergiloid E (4 and 5), were isolated and identified by comparing their spectroscopic data to literature values. Sphaeropsidin A (4), first isolated from *Aspergillus chevalieri*, is an established phytotoxin¹² that has recently gained interest as a cytotoxic agent, showing selectivity toward melanoma and kidney cancer cell lines with a unique mechanism of action targeting regulatory volume increase. Interestingly, the nearly isostructural aspergiloid E (5), recently reported by Yan et al., has no bioactivity associated with it. Our bioactivity testing supports this difference in activity and adds to the established structure—activity relationship studies.

■ RESULTS AND DISCUSSION

Isolated as an algal endophyte from the marine environment by BioViotica Naturstoffe GmbH, the A. porosus strain was provided to us for chemical analysis with a putative identification as a member of the Aspergillus family based on preliminary morphological analysis. Upon amplification and sequencing of the complete internal transcribed spacer (ITS) regions 1 and 2, using primers ITS1 and ITS4, 16 we could place the fungus into Aspergillus section Aspergillus (Figure S1, Supporting Information). The ITS region is highly conserved within this section, which required additional amplification of protein encoding regions, such as the partial β -tubulin (BenA), calmodulin (CaM), or RNA polymerase II second largest subunit (RPB2) genes for identification to the species level. 17 Phylogenetic analysis of the BenA region, amplified with primers Bt2a and Bt2b, 18 identified this strain as A. porosus (Figure S2, Supporting Information), a species recently described by Chen and co-workers.4

Compound 1 was isolated as a colorless oil (0.65 mg/L). The HRESIMS gave an m/z 459.2739 ([M + H]⁺), providing a molecular formula of $C_{27}H_{38}O_6$ (Δ ppm 0.4; calcd for $C_{27}H_{39}O_6$, 459.2741) with 9 degrees of unsaturation. The UV spectrum of 1 (CH₃CN) displayed maximum absorbances at 202 and 286 nm, indicating a conjugated system. Major bands in the IR spectrum of 1 include a broad band for a hydroxy group at 3390 cm⁻¹, a sharp strong carbonyl stretch at 1709 cm⁻¹, a strong band at 1645 cm⁻¹ indicative of an unsaturated ketone, and a strong band at 1606 cm⁻¹ correlating with a conjugated diene. The ¹³C NMR spectrum displayed three keto carbon atoms above 200 ppm, 10

aromatic or olefinic carbons atoms, and 13 aliphatic carbon atoms (Table 1). The 1H NMR spectrum of 1 exhibited two aromatic and two olefinic signals (5.5–7.0 ppm), one methoxy signal ($\delta_{\rm H}$ 3.71 ppm), two sets of diastereotopic methylene signals, four methine multiplets, three methyl singlets, and four methyl doublets.

Determination of the structure of 1 required 2D NMR correlation experiments including COSY, HMBC, and HSQC.

Table 1. ¹H and ¹³C NMR Spectroscopic Data for Compounds 1 and 2

	porosuphenol A (1)		porosuphenol B (2)		
position	δ_{C} , type	δ_{H} (J in Hz)	$\delta_{\rm C}$, type	$\delta_{ m H}$ (J in Hz)	
1	21.3, CH ₃	1.12, d (6.4)	21.4, CH ₃	1.09, d (6.3)	
2	71.7, CH	3.60, p (6.4)	71.8, CH	3.57, p (6.3)	
3	41.3, CH	2.52, dqd (9.8, 6.8, 6.4)	41.4, CH	2.50, dqd (10.0, 6.8, 6.3)	
4	142.3, CH	5.59, d (9.8)	141.5, CH	5.57, d (10.0)	
5	133.0, C		133.0, C		
6	146.1 CH	6.69, s	145.7, CH	6.98, s	
7	134.4, C		134.9, C		
8	201.9, C		200.9, C		
9	54.8, CH	3.97, q (6.9)	53.8, CH	4.53, q (6.9)	
10	212.1, C		212.3, C		
11	45.9, CH	2.80, dqd (8.7, 6.7, 6.2)	45.8, CH	2.90, dqd (8.3, 7.0, 6.0)	
12a	31.5, CH ₂	2.56, dd (13.8, 8.7)	29.6, CH ₂	2.62, dd (13.9, 6.0)	
12b		2.40, dd (13.8, 6.2)		2.45, dd (13.9, 8.3)	
13	119.0, C		119.3, C		
14	159.8, C		160.2, C		
15	98.7, CH	6.34, d (2.1)	98.7, CH	6.32, d (2.2)	
16	157.2, C		157.0, C		
17	110.4, CH	6.17, d (2.1)	110.3, CH	6.13, d (2.2)	
18	136.5, C		136.7, C		
19a	48.6, CH ₂	3.62, d (16.9)	48.8, CH ₂	3.72, d (16.9)	
19b		3.56, d (16.9)		3.57, d (16.9)	
20	206.9, C		207.0, C		
21	29.7, CH ₃	2.08, s	29.8, CH ₃	2.10, s	
22	16.2, CH ₃	1.03, d (6.8)	16.4, CH ₃	1.00, d (6.8)	
23	16.8, CH ₃	1.88, br s	16.9, CH ₃	1.88, br s	
24	13.3, CH ₃	1.84, br s	13.6, CH ₃	1.87, br s	
25	13.8, CH ₃	1.00, d (6.9)	14.1, CH ₃	1.14, d (6.9)	
26	17.3, CH ₃	0.95, d (6.7)	17.1, CH ₃	0.90, d (7.0)	
27	56.0, CH ₃	3.71, s	56.0, CH ₃	3.73, s	

Journal of Natural Products

Utilizing COSY, four distinct spin systems were constructed and connected with key HMBC correlations (Figure 1). The

Figure 1. Key COSY, HMBC (left), and NOE correlations (right) of 1 and 2.

trisubstituted double bond between C-4 ($\delta_{\rm C}$ 142.3 ppm) and C-5 ($\delta_{\rm C}$ 133.0 ppm) was supported by a long-range COSY correlation between H-4 and H-23 ($\delta_{\rm H}$ 5.59 and 1.88 ppm) along with HMBC correlations from H-3 ($\delta_{\rm H}$ 2.52 ppm) and H-23 to C-5. The second trisubstituted double bond (C-6/C-7; $\delta_{\rm C}$ 146.1/134.4 ppm) was placed by a long-range COSY correlation between H-6 and H-24 ($\delta_{\rm H}$ 6.69 and 1.84 ppm), along with an HMBC correlation from H-24 to C-7 ($\delta_{\rm C}$ 134.4 ppm). HMBC correlations between H-4 and H-23 to C-6 ($\delta_{\rm C}$ 146.1 ppm) and from H-6 and H-24 to C-8 ($\delta_{\rm C}$ 201.9 ppm) supported the attachment of the double bonds to the carbonyl group at C-8 and fully described the dieneone moiety. The isolated H-9/H-25 spin system could be placed between the 1,3-diketone moiety due to the deshielded signal of H-9 ($\delta_{\rm H}$ 3.97 ppm) along with HMBC correlations from H-25 ($\delta_{\rm H}$ 1.00 ppm) to C-8 and C-10 ($\delta_{\rm C}$ 201.9 and 212.1 ppm). The final H-11/H-12/H-26 spin system could be linked to C-10 by the HMBC correlations from H-26, H-12a, and H-12b ($\delta_{\rm H}$ 2.56 and 2.40 ppm) to C-10, thus completing the side chain. HMBC correlations from H-21 ($\delta_{\rm H}$ 2.08 ppm) to C-20 and C-19 ($\delta_{\rm C}$ 206.9 and 48.6 ppm) confirmed an acetonyl moiety. The benzenediol core consisted of four aromatic carbons (δ_C 119.0, 98.7, 110.4, and 136.5 ppm) and two oxygenated aromatic carbons (δ_C 159.8 and 157.2 ppm). A long-range COSY (I = 2.1 Hz) correlation between H-15 and H-17 (δ_{H} 6.34 and 6.17 ppm) required that these protons are meta to one another. Strong HMBC correlations from H-15 to C-13 and C-17 ($\delta_{\rm C}$ 119.0 and 110.4 ppm) along with correlations from H-17 to C-13 and C-15 ($\delta_{\rm C}$ 119.0 and 98.7) further supported the assignment proposed. The methoxy group ($\delta_{\rm H}$ 3.71 ppm) was placed at C-14 ($\delta_{\rm C}$ 159.8 ppm) due to its HMBC correlation. HMBC correlations from the methylene H-12a/H-12b to C-14 ($\delta_{\rm C}$ 159.8) and C-18 ($\delta_{\rm C}$ 136.5) support the placement of the side chain next to the methoxy group. The acetonyl moiety was located meta to the methoxy group due to HMBC correlations from H-19a/H-19b ($\delta_{
m H}$ 3.62/3.56 ppm) to C-13 and C-17 in 1.

The double-bond geometry of 1 was established from NOE experiments. The C-4/C-5 double bond was determined as *E* based on three NOE correlations that were observed: H-4/H-6, H-23/H-3, and H-23/H-22 (Figure 1). The C-6/C-7 double bond was also assigned *E* as shown by NOE correlations between H-4/H-24, H-6/H-9, and H-6/H-25 (Figure 1).

With four asymmetric carbon centers and a flexible linear side chain, assigning the absolute configuration of 1 proved to be a difficult task. The secondary alcohol was accessible to Mosher ester analysis ¹⁹ by separately reacting 1 with both R and S α -methoxy- α -trifluoromethylphenylacetic (MTPA) acid chlorides to give the 1S and 1R MTPA esters, respectively.

Comparative analysis of the ¹H NMR spectra of both MTPA esters assigned unequivocally C-2 as being *S* configured (Figure 2 and Figure S28, Supporting Information). With the

Figure 2. $\Delta \delta_{S-R}$ values for MTPA esters of 1 (1S and 1R). Experimental ${}^3f_{(H-H)}$ and ${}^{2-3}f_{(C-H)}$ values of 1 and 2 leading to assignment of the rotamer equilibrium between A1 and A2.

absolute configuration of the secondary alcohol established, a *I*-based conformational analysis²⁰ was used to determine the configuration of the vicinal methyl group (C-22). Due to the medium magnitude of the ${}^{3}J_{(H2-H3)}$ coupling constant (6.4) Hz), an equilibrium of conformers must be considered.²⁰ Out of the six possible pairs of conformers (3-erythro; 3-threo) (Figure S32, Supporting Information), the A1/A2 equilibrium was the only one with the expected coupling constants that matched the $^{2-3}J_{(C-H)}$ coupling constants measured from a HETLOC²¹ spectrum (Figure 2). This supported a threo relationship between H-2 and H-3, making the absolute configuration 3S. To save precious material, the remaining two asymmetric centers were assigned by the loss-free comparative analysis of computed and experimental spectroscopic data, including ¹H and ¹³C chemical shifts, coupling constants, NOE distances, UV, and electronic circular dichroism (ECD) spectra. A discussion of the computational analysis performed is presented below.

Compound **2** was isolated as a colorless oil and was found to have an identical mass and molecular formula of $C_{27}H_{38}O_6$ ([M + H]⁺, m/z 459.2738; Δ ppm 0.7; calcd for $C_{27}H_{39}O_6$, 459.2741) compared to **1**. Similar UV, IR, and NMR data (Table 1) indicate that **2** is a stereoisomer (Figure 1). The double-bond geometry was examined with NOE experiments, and both double bonds were established as E, supporting a diastereomeric relationship between **1** and **2**.

Deuterium exchange studies were used to establish the stereochemical relationship between 1 and 2. DCl was added to a solution of 1, and the mixture was monitored by ¹H NMR spectroscopy. Once equilibrated, the ¹H NMR spectrum showed a mixture of 1 and 2 (1.4:1), with the signal corresponding to H-9 clearly diminished as expected from the acidic proton H-9 in a 1,3 diketo system (Figure 3). This was used to establish 1 and 2 as C-9 epimers and supports the absolute configuration as S for both C-2 and C-3 of 2. The lower pH in the fungal culture (pH 5.5) could be responsible for production of both diastereomers. This stereochemical relationship was further supported by the Mosher ester analysis of 1 and by the ${}^3J_{(\text{H2-H3})}$ and ${}^{2-3}J_{(\text{C-H})}$ values of 2 being almost identical to those observed in 1 (Figure 2). The remaining two asymmetric centers for both 1 and 2 were assigned by comparison of quantum mechanics (QM)-calculated NMR and ECD spectra.

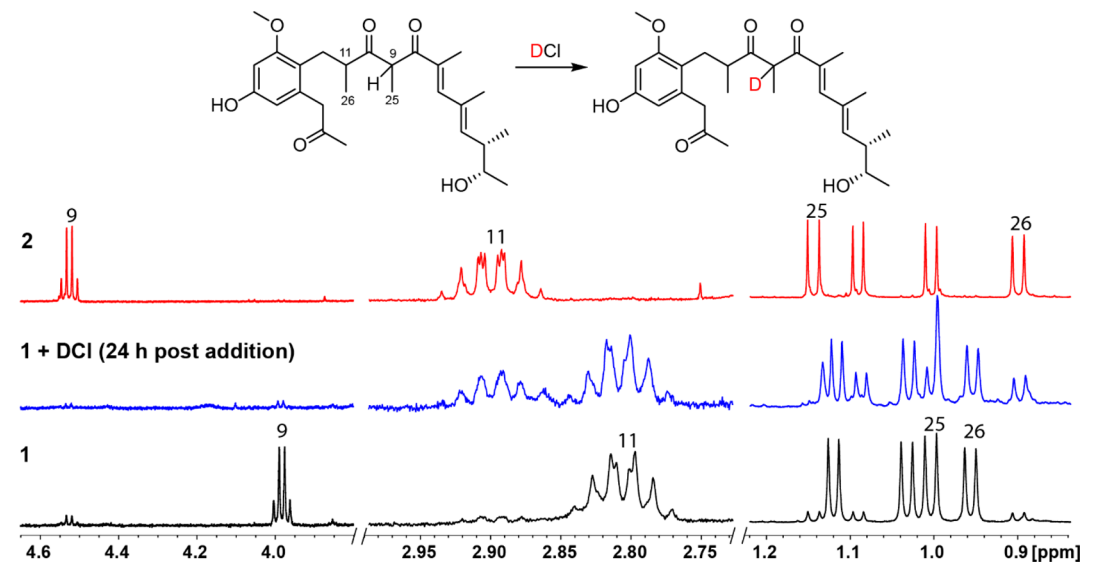


Figure 3. Key regions of the ¹H NMR spectrum of a deuterium-exchange study using compound 1.

To determine the absolute configuration for the porosuphenols, computational methods were used to predict chiroptical properties (ECD) and chemical shift predictions of candidate structures. A standard pipeline was used initially for performing this analysis: (1) a library of conformers was created using automatic sampling tools based on molecular mechanics calculations; (2) density functional theory (DFT) calculations were applied to determine optimized geometries, free energies, and NMR shielding tensors for NMR chemical shift predications; (3) Boltzmann averages of NMR shift data were assembled, and computed chemical shifts and ECD spectra were compared to experimental data.

An initial conformational analysis of the four possible configurations (2S,3S,9R,11R; 2S,3S,9S,11R; 2S,3S,9R,11S; 2S,3S,9S,11S) was performed using Spartan and the MMFF force field. The subsequent reoptimization of the conformers was done with the hybrid density functional B3LYP with the 6-31+G* basis set. Conformers within an energy range of 3 kcal/mol were further processed with the hybrid WP04 functional for computation of high-accuracy proton chemical shifts. The results from these computations excluded the configurations 2S,3S,9R,11S and 2S,3S,9S,11S for 1 and 2 (Table 2), with

Table 2. CMAE for Compounds 1 and 2 Compared with NMR Isotropic Shift Values Computed at the WP04/aug-cc-pVDZ Level with Chloroform IEFPCM Solvation

	2S,3S,9R,11R	2S,3S,9S,11R	2S,3S,9R,11S	2S,3S,9S,11S
CMAE 1	0.14	0.10	0.18	0.19
CMAE 2	0.13	0.16	0.20	0.23

2S,3S,9S,11R providing a corrected mean absolute error (CMAE) of 0.10 for 1 and 2S,3S,9R,11R providing a CMAE of 0.13 for 2. This result agreed with the deuterium-exchange study that established 1 and 2 as C-9 epimers.

Since it is desirable and good practice to support assignments with multiple lines of evidence, are the ECD spectra were computed for each possible configuration of 1 and 2. Time-dependent (TD)DFT calculations of ECD spectra of the 2S,3S,9R,11R-configured diastereomer at the CAM-B3LYP/TZVP level with integral equation formalism PCM

(IEFPCM) in acetonitrile provided a good match for the experimental spectra of 2 with a $\Delta_{ESI} = 0.9059$ (Figure 4),

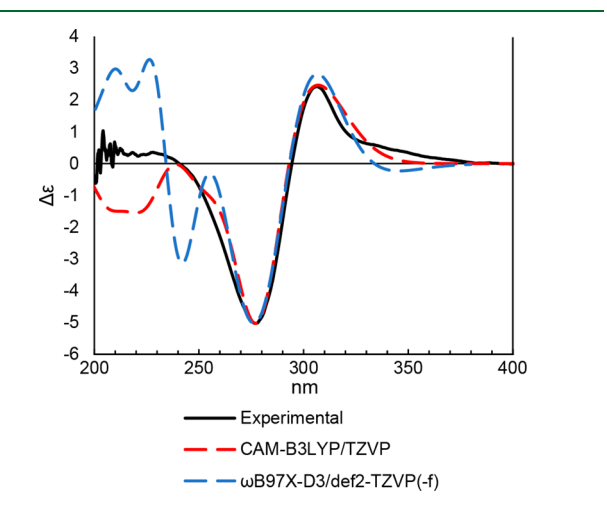


Figure 4. Experimental ECD spectra of **2** in acetonitrile with the computed 2*S*,3*S*,9*R*,11*R* diastereomer. Red dotted line: CAM-B3LYP/TZVP (shift: 6 nm; σ = 0.25 eV; $\Delta_{\rm ESI}$ = 0.9059); blue dotted line: ω B97X-D3/def2-TZVP(-f) (shift: 20 nm; σ = 0.3 eV; $\Delta_{\rm ESI}$ = 0.8165).

providing further support for this as the correct configuration. In addition, $\omega B97X-D3/def2-TZVP(-f)$ gave a similar curve, showing that the functionals used were well-suited for the ECD calculations.

Interestingly, none of the computed ECD spectra of any tested configuration (2S,3S,9R,11R; 2S,3S,9S,11R; 2S,3S,9R,11S; or 2S,3S,9S,11S) produced a good fit with the experimental ECD spectrum for 1. However, with confidence gained in the computational assignment of ECD and NMR shifts for 2 and the knowledge from the deuterium-exchange experiments that 1 had to be the C-9 epimer of 2, the conformational analysis for 1 was revisited and the dispersion-corrected B3LYP-D3 method was used to re-evaluate the conformational ensemble. At the same time, the automatic sampling process in Spartan was revisited, and indeed additional conformations were found of the C-9 enantiomer,

Table 3. NOE Distances and Coupling Constants Used as Constraints in Stereofitter, alongside Computed Averages for Each
Conformer Ensemble and γ^2 Values for Each Ensemble

	exptl	2S,3S,9R,11R	2S,3S,9S,11R	2S,3S,9R,11S	2S,3S,9S,11S
NOE _{H6, H9} (Å)	2.1	2.3	2.2	1.9	2.0
$NOE_{H6, H4}$ (Å)	2.6	2.7	2.6	2.9	2.6
$NOE_{H6, Me23}$ (Å)	3.0	2.8	3.0	2.9	2.9
$NOE_{H6, Me26}$ (Å)	3.5	3.8	3.9	3.3	3.8
$^{3}J_{H2, H3}(Hz)$	6.4	6.3	6.1	6.5	6.1
$^{3}J_{\text{Mel, H3}}(\text{Hz})$	2.2	1.7	2.1	3.6	2.4
$^{3}J_{\text{Me22, H2}}(\text{Hz})$	4.7	3.5	4.1	3.8	3.3
χ^2		5.7	4.4	5.5	4.6

which were not originally included. This highlights the need to thoroughly review the conformational space, rather than use automatic tools as black box approaches.

Closer analysis of the low-energy conformers comprising the Boltzmann distributions based on the DFT energies for 1 revealed that none of the significantly populated conformers exhibited an *anti*-configuration between H-2 and H-3 (Figures 2 and 5). To yield the averaged 6.4 Hz $^3J_{(H2-H3)}$ coupling constant observed experimentally for compound 1, an approximate 3:2 ratio of *anti:gauche* conformers must be present. Even single-point energy calculations using implicit solvent effects (CPCM, PCM) with and without dispersion at a number of levels of theory (M06-2X, B3LYP-D3, B3LYP) and coupled-cluster calculations using DLPNO-CCSDT/def2-TZVP²⁴ (Table S1, Supporting Information) failed to produce a conformer ensemble that reflected the experimentally observed spectra for 1.

Based on these results, it appeared that conformational flexibility and an accumulation of small effects prevented efforts to construct an accurate conformer ensemble for compound 1 by computational methods. Approximations for dispersion and solvent effects significantly changed the energy of single conformers and yielded very different conformer ensembles. In the presented study, dispersion slightly overestimated hydrogen bonds, but the DLPNO-CCSDT results more or less confirmed the energetic order found with the DFT-D3 method. Similarly, addition of implicit solvent effects significantly changed the energetic order of conformers even with the coupled-cluster method, but did not produce an ensemble consistent with NMR data. It is possible that ab initio construction of an accurate conformer ensemble for 1 may require consideration of explicit solvent effects, which would be prohibitively intensive computationally.

As an alternative, it was examined as to whether the conformer search could be guided by the experimental NMR data. Stereofitter (Mestrelab)^{3a} was used to sample conformers based on experimental ${}^{3}J_{(C-H)}$ coupling constants and NOEderived distances of 1 to more accurately model the conformation of the side chain. From the HETLOC spectra recorded in the *J*-based conformational analysis, ${}^{3}J_{(H2-H3)}$, ${}^{3}J_{\text{(Me1-H3)}}$, and ${}^{3}J_{\text{(Me22-H2)}}$ were used as constraints for the terminal end of the side chain. In addition to this, NOE distances between H-6/H-9, H-6/H-4, H-6/Me-26, and H-6/ Me-23 were obtained using the peak amplitude normalization for improved cross-relaxation (PANIC) approach.²⁵ Briefly, fully relaxed 1D PFGSE NOE spectra²⁶ with zero-quantum suppression²⁷ were recorded with varying mixing times. PANIC plots (integral ratio of NOE peak to inverted peak plotted against mixing time, Figure S30, Supporting Information) were then used to obtain the cross-relaxation

rate constants, from which accurate NOE distances were obtained. ²⁸ Combining these NOE distances with the abovementioned coupling constants provided experimental evidence for the conformation of the side chain. Next, these NOE-derived distances and $^3J_{\rm HH}$ and $^3J_{\rm CH}$ couplings (Table 3) were used as constraints to generate conformer ensembles. In each instance, Stereofitter provided combinations of two conformers (Figure 5, Table S2, Supporting Information) that best fit the

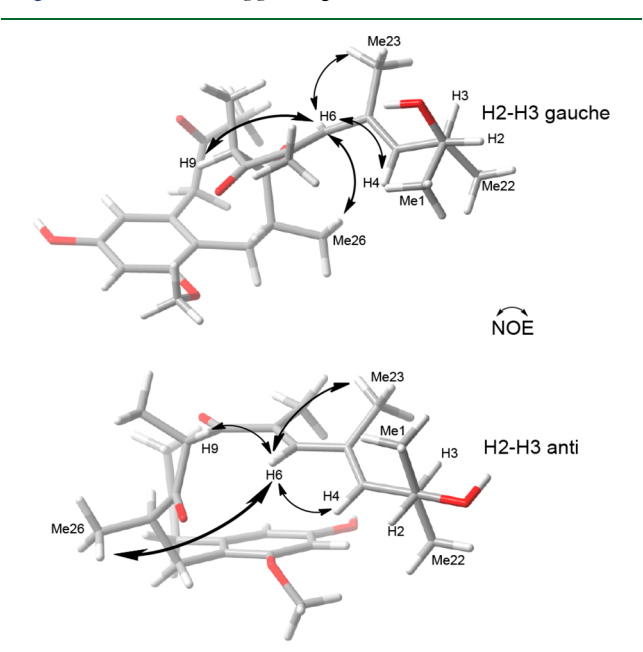


Figure 5. Two best 2*S*,3*S*,9*S*,11*R* conformers for 1 resulting from Stereofitter analysis with NOE and coupling constant constraints.

NOE distances and J values. Of the four configurations, 2S,3S,9S,11R provided the best χ^2 values for J and NOE distance values (Table 3) for 1. Computation of ECD spectra for this ensemble at the ω B97XD/def2-TZVP level with conductor-like PCM (CPCM) in acetonitrile provided a good match for the experimental spectra, with a $\Delta_{\rm ESI}=0.9221$ (Figure 6). This established the absolute configuration of 1 as 2S,3S,9S,11R, which was in full agreement with our NMR data and deuterium-exchange results obtained.

Further chemical analysis efforts resulted in the isolation of compound 3, a colorless oil with m/z 445.2572 ([M + H]⁺) in the HRESIMS. This was 14 mass units less than 1 and corresponded to a molecular formula of $C_{26}H_{36}O_6$ ($\Delta ppm = 2.8$; calcd for $C_{26}H_{37}O_6$, 445.2580). The UV spectrum of 3 (30% CH_3CN-H_2O) was only slightly shifted from that of 1, with maxima at 210 and 289 nm, implying a similar structure. When a 1H NMR spectrum was recorded in d_3 -acetonitrile, 3

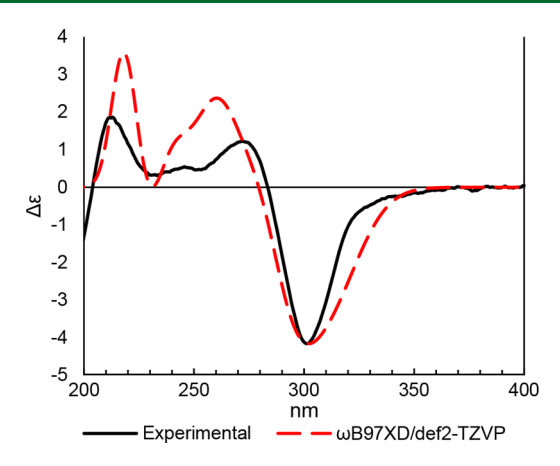


Figure 6. Experimental ECD spectrum of **1** in acetonitrile with computed spectra of the 2*S*,3*S*,9*S*,11*R* diastereomer. Red dotted line: ω B97XD/def2-TZVP (shift: -1 nm; $\sigma = 0.22$ eV; $\Delta_{ESI} = 0.9221$).

proved to be a mixture of two compounds (Figure 7) in a 1:1.35 ratio. After recording the 2D NMR spectra, including COSY, HMBC, and HSQC, the minor component, $\bf 3a$ (porosuphenol C) could be determined as the 14-desmethyl analogue of $\bf 1$ (Figure 8). With nearly identical correlations, the distinguishing feature of $\bf 3b$ (porosuphenol D) was a ring closure, as evident by HMBC correlations from H-12a/H-12b, H-25, and H-26 to C-10 with a chemical shift of $\delta_{\rm C}$ 102.7 in $\bf 3b$ but $\delta_{\rm C}$ 212.4 in $\bf 3a$ (Table 4). This is a result of a nucleophilic attack by the phenol on C-14 to the C-10 carbonyl group in $\bf 3a$, generating the hemiketal $\bf 3b$. While both isomers are easily separated via preparative HPLC, the hemiketal formation/opening occurred within minutes, always resulting in a mixture of $\bf 3a$ and $\bf 3b$. Due to rapid epimerization alongside the

Figure 8. Key COSY and HMBC correlations of 3a and 3b.

ketone—hemiketal equilibrium, attempts to assign the configuration of compound 3 were unsuccessful.

All compounds isolated from *A. porosus* were tested for biological activity in antibacterial (*S. aureus*, ATCC 25923; *S. aureus*, ATCC BAA-41) and cytotoxicity assays (colon carcinoma HCT-116, ATCC CCL-247). Interestingly, only sphaeropsidin A (4) showed significant activity (Table 5), despite the nearly identical structure to aspergiloid E (5), as previously reported. The only structural difference between these two diterpenoids is a hydroxy group at C-9 in 4, compared to a methine in 5. Although both structures contain a reactive Michael acceptor and a labile hemiketal, the inactivity of 5 might indicate that these shared functional groups are not the sole cause of bioactivity even if these

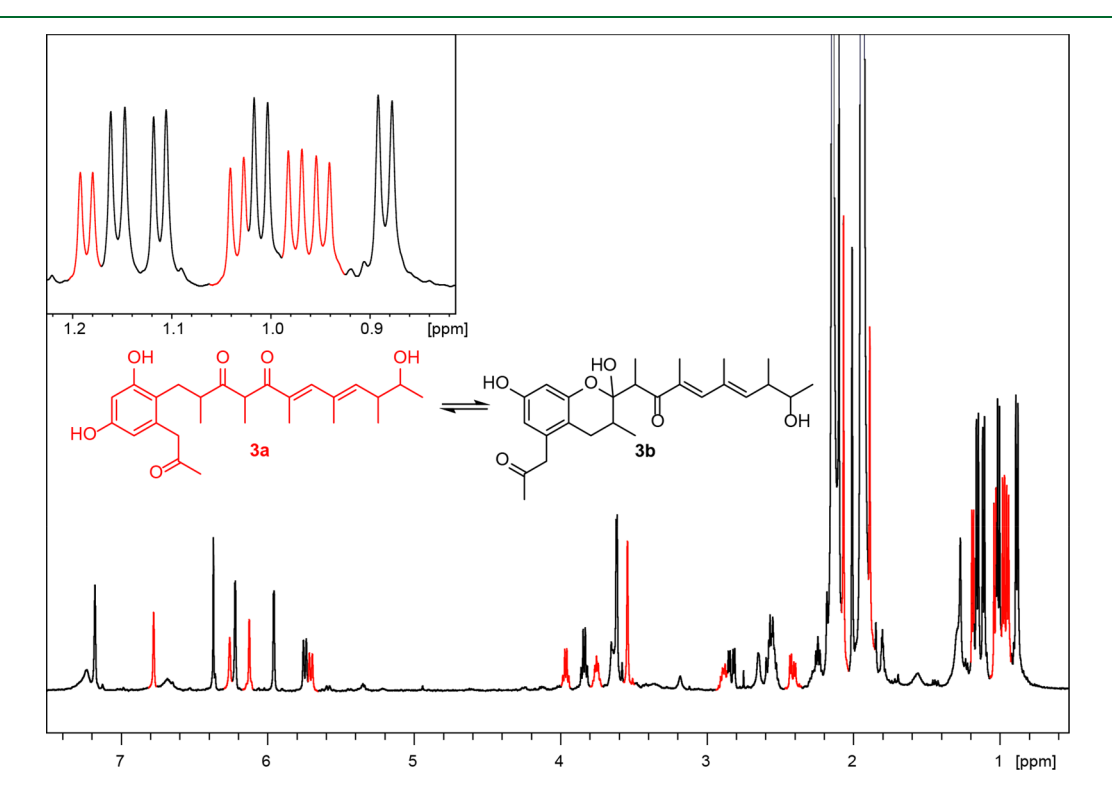


Figure 7. ¹H NMR spectra of 3a and 3b in d_3 -acetonitrile.

Table 4. ¹H and ¹³C NMR Spectroscopic Data for Compounds 3a and 3b

	porosuphenol C (3a)		porosuphenol D (3b)	
position	$\delta_{\rm C}$, type	$\delta_{ m H}$ (J in Hz)	$\delta_{\rm C}$, type	δ_{H} (J in Hz)
1	21.7, CH ₃	1.19, d (6.3)	21.1, CH ₃	1.11, d (6.3)
2	72.4, CH	3.75, dq (6.3, 5.7)	71.4, CH	3.65, m ^a
3	40.9, CH	2.55, dqd (9.9, 6.7, 5.7)	41.0, CH	2.55, m ^a
4	143.6, CH	5.71, d (9.9)	142.0, CH	5.75, d (9.9)
5	а		а	
6	146.8, CH	6.78, s	146.8, CH	7.18, s
7	134.2, C		135.3, C	
8	202.1, C		210.8, C	
9	54.5, CH	3.96, q (6.8)	41.5, CH	3.84 q (7.1)
10	212.4, C		102.7, C	
11	45.6, CH	2.89, dqd (9.2, 6.6, 5.7)	31.1, CH	2.24, m
12a	31.7, CH ₂	2.42, dd (13.6, 5.7)	26.6, CH ₂	2.83, dd (15.8, 5.9)
12b		2.57, dd (13.6, 9.2)		2.16, m ^a
13	117.2, C		112.4, C	
14	157.0, C		154.0, C	
15	102.3, CH	6.26, s	102.9, CH	5.96, br s
16	а		а	
17	110.3, CH	6.13, s	111.3, CH	6.22, br s
18	137.1, C		137.0, C	
19a	48.6, CH ₂	3.54, s	48.3, CH ₂	3.64, d (16.7)
19b				3.60, d (16.7)
20	207.0, C		206.8, C	
21	29.6, CH ₃	2.07, s	29.5, CH ₃	2.10, s
22	17.2, CH ₃	1.03, d (6.7)	16.8, CH ₃	1.01, d (6.8)
23	16.5, CH ₃	1.94, s ^b	16.6, CH ₃	1.93, s ^b
24	13.0, CH ₃	1.89, s	13.4, CH ₃	2.01, s
25	13.6, CH ₃	0.98, d (6.8)	14.0, CH ₃	1.15, d (7.1)
26	17.0, CH ₃	0.95, d (6.6)	14.9, CH ₃	0.88, d (7.0)
^a Overlapped peaks. ^b Under residual solvent peak.				

Table 5. Bioactivity of Sphaeropsidin A (4) and Aspergiloid E (5)

	IC_{50} (μ M)		
	sphaeropsidin A (4)	aspergiloid E (5)	
S. aureus (ATCC 25923)	32.6 ± 1.3	71.6 ± 5.2	
S. aureus (ATCC BAA-41)	35.3 ± 1.5	77.8 ± 5.4	
P. aeruginosa (ATCC 15442)	>100	>100	
HCT-116 (ATCC CCL-247)	4.9 ± 0.4	32.7 ± 2.3	

^aPositive controls: *S. aureus* ATCC 25923, *P.aeruginosa* ATCC 15442: 100% growth inhibition with 0.125 mg/mL kanamycin; *S. aureus* ATCC BAA-41: 100% growth inhibition with 0.125 mg/mL vancomycin. HCT-116 ATCC CCL-247: 82.8% cell growth inhibition with 200 μ M etoposide.

functional groups may be considered PAINS.²⁹ It was also observed that **5** is less stable than **4**; when left in MeOD, **5** will form a mixture of methanol adducts, while **4** remains stable. The porosuphenols A, B, and C/D (**1**, **2**, **3a**, and **3b**) were inactive in antibacterial and cell viability assays, and no activity was observed for antifungal, antimalaria,³⁰ antitubercular,³¹ antioxidant, and metal-chelating activity (>50 μ M).

The present study presents a survey of the chemical structures and bioactivity of the algal endophyte *A. porosus*. This strain produces a diversity of secondary metabolites, consistent with previous studies that have found marine fungi

are underexplored compared to terrestrial fungi and that marine plant-associated fungi are an especially rich source for metabolites. Four new metabolites, named porosuphenols A-D (1, 2, 3a, and 3b), and two known diterpenes (4 and 5) were isolated and their structures derived from extensive MS and NMR experiments. To establish the absolute configuration of these flexible polyketides, Mosher ester analysis was used combined with a *I*-based conformational analysis, DFT-based computations of spectroscopic, and chiroptical data in comparison with experimental data. Initially, using the hybrid WP04 functional to compute ¹H NMR chemical shifts provided results that agreed with a deuterium-exchange study in that 1 and 2 are C-9 epimers. However, while computed ECD spectra provided a good fit for 2 as 2S,3S,9R,11R, none of the other configurations were a good fit for compound 1. Further investigation revealed that the construction of the conformer ensemble was highly sensitive to a number of small effects. A refined conformational search guided by experimental NMR parameters was required to determine the absolute configuration of 1 as 2S,3S,9S,11R, with best fit for all experimental parameters including ${}^{3}J_{(H-H)}$ and ${}^{3}J_{(C-H)}$ coupling constants, NOE distances, ¹H NMR chemical shifts, and ECD spectra. An unusual case of structures for which standard DFTbased conformational sampling failed for one specific configuration has been presented, most probably due to explicit solvent effects, and a solution using Stereofitter with implemented experimentally derived parameters was applied to yield the correct conformers for 1. The structure of 3a/3b was derived from MS and NMR experiments to be a 14-desmethyl derivative; however, due to rapid equilibrium between 3a and 3b, the linear and ring-closed isomers, the absolute configuration was not determined.

■ EXPERIMENTAL SECTION

General Experimental Procedures. Optical rotations were recorded on a JASCO P-1010 polarimeter. UV spectra were recorded on a BioRad SmartSpec3000. IR spectra were recorded on a Thermo Scientific Nicolet 6700 FT-IR spectrometer. ECD spectra were recorded on a JASCO J-1000 spectrometer. NMR spectra were acquired on a Bruker Avance III 500 MHz, a Bruker Avance III 700 MHz, or a Bruker Avance III 800 MHz spectrometer equipped with a 5 mm TXI probe or 5 mm BBO probe (500 and 700 MHz), TCI cryoprobe (700 MHz), or TXI cryoprobe (800 MHz), with the residual solvent used as an internal standard (CDCl₃: 7.26/77.16; CD₃CN: 1.94/118.26). Low-resolution ESIMS and HRTOFMS (ESI+) mass spectra were recorded on an Agilent 1100 series LC with MSD 1946 and an Agilent 1200 series LC with 6230 TOF MS, respectively. A Teledyne Isco CombiFlash Companion system was used for adaptive gradient, automated flash chromatography. Analytical HPLC was performed using an Agilent 1100 HPLC system equipped with a photodiode array detector. The mobile phase consisted of ultrapure water (A) and CH₃CN (B) with 0.05% formic acid in each solvent. A gradient method from 10% A to 100% B in 35 min at a flow rate of 0.8 mL/min was used. The column (Phenomenex Kinetex C_{18} , 5 μ m × 150 mm × 4.6 mm) was reequilibrated before each injection, and the column compartment was maintained at 30 °C throughout each run. Semipreparative HPLC (Phenomenex Kinetex C_{18} , 5 μ m × 150 mm × 10 mm) utilized isocratic elution conditions or a gradient system with a flow rate of 4 mL/min on an Agilent 1100 HPLC system operating at room temperature equipped with a photodiode array detector. Preparative HPLC (Phenomenex Luna C_{18} , 5 μ m × 250 mm × 21 mm) was conducted at room temperature, using isocratic elution conditions or a gradient system with a flow rate of 20 mL/min utilizing an Agilent 1260 Infinity series HPLC equipped with a DAD detector. All samples were filtered through a 0.45 μm nylon filter or centrifuged at 14 000

rpm for 5 min before LC/MS and HPLC analysis. Analytical thin-layer chromatography (TLC) was performed on precoated silica gel 60 F_{254} plates (Eppendorf). TLC plates were visualized by UV (254 and 360 nm) and by spraying with anisaldehyde solution followed by heating at 80 $^{\circ}\text{C}.$ General reagents were from Sigma-Aldrich and VWR International.

Identification of Fungal Species. The endophytic fungus Aspergillus sp., strain G23, was obtained from Bioviotica. Phylogenetic identification of the fungal strain was achieved by PCR amplification and sequencing of both the ITS and partial beta-tubulin encoding genes of DNA, according to a published procedure. ITS 1 forward primer and ITS4 reverse primer were used to amplify the complete ITS sequence, while Bt2a forward primer and Bt2b reverse primer were used to amplify the partial beta-tubulin encoding gene. The closest match for the beta-tubulin gene fragment from a nucleotide megaBLAST was Aspergillus porosus (strain CBS 1417700) with 96% sequence coverage and 100% identity (GenBank: LT671130.1). The beta-tubulin gene fragment was required to further distinguish within Aspergillus section Aspergillus; see the phylogenetic trees.

The phylogeny was inferred by using the maximum likelihood method (Tamura three-parameter model³³ for ITS and Kimura twoparameter model³⁴ for partial beta tubulin gene fragment). The trees with the highest log likelihood (ITS = -862.4657; beta tubulin = -1353.3207) are shown (Figures S1 and S2, Supporting Information). Initial tree(s) for the heuristic search were obtained automatically by applying Neighbor-Join and BioNJ algorithms to a matrix of pairwise distances estimated using the maximum composite likelihood (MCL) approach and then selecting the topology with superior log likelihood value. The trees are drawn to scale, with branch lengths measured in the number of substitutions per site. The analysis involved 26 nucleotide sequences for ITS and nine for beta tubulin, all retrieved from GeneBank³⁵ or the NCBI BLAST targeted loci sequences from the fungi type and reference material collection.³⁶ All positions with less than 95% site coverage were eliminated. Accordingly, fewer than 5% alignment gaps, missing data, and ambiguous bases were allowed at any position. There was a total of 458 positions in the final data set for the ITS region and 295 for the beta tubulin. Phylogenetic analyses were conducted in MEGA7.

Extraction and Isolation. All fungal cultures were extracted with 10 L of ethyl acetate with shaking/stirring overnight after separation of fungal mycelia from culture broth by filtration. The organic layer was separated and washed with 10 L of H₂O before evaporation to dryness in vacuo. The culture broth was then treated with XAD-7 resin and left overnight. XAD-7 resin was separated by filtration, washed with 2 L of DI-water, and then extracted with 2 L of 1:1 acetone-methanol mixture. The organic extract was concentrated before partitioning between ethyl acetate and water. In turn, the aqueous layer was washed three times with ethyl acetate. The organic layers were combined, dried, and concentrated in vacuo. The organic extract of a 10 L culture in 1158 medium (malt extract 20 g/L; Dglucose 10 g/L; yeast extract 2 g/L; NH₄HSO₄ 0.5 g/L; pH 6.0) was separated into seven fractions by normal-phase vacuum-liquid chromatography (VLC) eluted with a CH2Cl2 to MeOH gradient. Altogether, 6.5 mg of porosuphenol A (1), 5.0 mg of porosuphenol B (2), and a combined 3.0 mg of porosuphenols C and D (3a and 3b) were isolated from fraction 5.

Porosuphenol A (1): colorless oil; $[\alpha]^{21}_{D}$ –130.8 (c 0.1, CH₃CN); IR (ATR) ν_{max} 3390, 2970, 2932, 1709, 1645, 1606, 1457, 1358, 1307, 1276, 1198, 1149, 1086, 1022, 833; ECD (c 0.1, CH₃CN) 194.3 (–2.3), 215.4 (+1.7), 234.4 (+0.3), 245.3 (+0.5), 255.1 (+0.6), 274.6 (+1.2), 299.9 (–4.7); UV (c 0.1, CH₃CN) λ_{max} (log ε) 204 (4.2), 285 (3.8) nm; ¹³C NMR (176 MHz, CH₃CN- d_3) and ¹H NMR (700 MHz, CH₃CN- d_3) see Table 1; HRESIMS m/z 459.2739 [M + H]⁺ (calcd for C₂₇H₃₉O₆(+1) 459.274; Δppm = 0.4).

Porosuphenol B (2): colorless oil; $[\alpha]^{21}_{D}$ –35.8 (c 0.1, CH₃CN); IR (ATR) ν_{max} 3362, 2969, 2931, 1708, 1646, 1606, 1457, 1357, 1308, 1277, 1198, 1149, 1087, 1022, 832; ECD (c 0.1, CH₃CN) 192.6 (–1.9), 204.5 (+0.8), 221.2 (+0.2), 230.5 (+0.3), 277.5 (–5.0), 306.2 (+2.4); UV (c 0.1, CH₃CN) λ_{max} (log ε) 203 (4.2), 285 (3.8) nm; ¹³C NMR (176 MHz, CH₃CN- d_3) and ¹H NMR (700 MHz, CH₃CN- d_3)

see Table 1; HRESIMS m/z 459.2738 [M + H]⁺ (calcd for $C_{27}H_{39}O_6(+1)$ 459.274; Δ ppm = 0.7).

Porosuphenol C (3a): colorless oil; $[\alpha]^{21}_{D}$ –39.8 (c 0.1, CH₃CN); IR (ATR) ν_{max} 3343, 2971, 2931, 1700, 1620, 1456, 1355, 1329, 1232, 1144, 1126, 1053. 1027, 1004, 939, 921; UV (30% CH₃CN-H₂O) λ_{max} 210, 288 nm; ³⁸ ¹³C NMR (176 MHz, CH₃CN-d₃) and ¹H NMR (700 MHz, CH₃CN-d₃) see Table 4; HRESIMS m/z 467.2392 [M + Na]⁺ (calcd for C₂₆H₃₆O₆Na(+1) 467.24; Δppm = 2.8).

Porosuphenol D (3b): colorless oil; $[\alpha]^{21}_{\rm D}$ –39.8 (c 0.1, CH₃CN); IR (ATR) $\nu_{\rm max}$ 3343, 2971, 2931, 1700, 1620, 1456, 1355, 1329, 1232, 1144, 1126, 1053. 1027, 1004, 939, 921; UV (30% CH₃CN-H₂O) $\lambda_{\rm max}$ 210, 288 nm; ¹³C NMR (176 MHz, CH₃CN-d₃) and ¹H NMR (700 MHz, CH₃CN-d₃) see Table 4; HRESIMS m/z 467.2392 [M + Na]⁺ (calcd for C₂₆H₃₆O₈Na(+1) 467.24; Δppm = 2.8).

Preparation of (R)- and (S)-MTPA Ester Derivatives of **Porosuphenol A (1).** Compound 1 (0.88 mg, 1.91 \times 10 μ mol) was dissolved in 100 μ L of dry acetonitrile. To this was added pyridine (3.0 μ L, 37.4 μ mol) dissolved in 100 μ L of dry acetonitrile, followed by (S)-(+)- α -methoxy- α -(trifluoromethyl)phenylacetyl (MTPA) chloride, dissolved in 100 μ L of dry acetonitrile. The reaction was monitored by TLC. After 24 h, the reaction was quenched with H₂O and extracted with ethyl acetate. The organic layers were combined, dried with MgSO₄, and concentrated to dryness under reduced pressure. The desired product, the (R)-MTPA (1R) ester of porosuphenol A, was purified by HPLC, and its structure determined using one- and two-dimensional NMR techniques. Selected ¹H NMR data of 1R (800 MHz, CH₃CN- d_3): δ 5.43 (1H, d, I = 9.8 Hz, H-4), 5.08 (1H, p, J = 6.4 Hz, H-2), 2.80 (1H, dqd, J = 9.8, 6.8, 6.4 Hz, H-2)3), 1.36 (3H, d, J = 6.4 Hz, H-1), 0.95 (3H, d, J = 6.8 Hz, H-22). In an analogous manner, 1 (0.88 mg, 1.91 \times 10 μ mol) was converted with (R)-MTPA chloride to yield the (S)-MTPA (1S) ester of porosuphenol A. Key ¹H NMR shifts of **1S** (800 MHz, CH₃CN- d_3): δ 5.53 (1H, d, J = 9.6 Hz, H-4), 5.10 (1H, p, J = 6.4 Hz, H-2), 2.89 (1H, dqd, J = 9.8, 6.8, 6.4 Hz, H-3), 1.28 (3H, d, J = 6.4 Hz, H-1),1.09 (3H, d, I = 6.8 Hz, H-22).

Deuterium-Exchange Study. To an NMR tube containing a solution of 1 (1 mg, 3.6 mM) in CH₃CN- d_3 was added DCl (3 μ L of 2% w/w in D₂O). The NMR tube was inverted to mix the sample and then monitored by 1 H NMR spectroscopy for 24 h.

Accurate NOÉ Distances. A sample of 1 was dissolved in CH_3CN-d_3 (2.5 mg, 9.1 mM), and several 1D PFGSE NOE spectra with zero-quantum suppression were obtained, ²⁶ using the Bruker pulse program selnogpzs.2, with 5 s D1 to ensure complete relaxation (T_1 was measured as 1 s using the inversion—recovery method). For each distance to be determined, seven NOE experiments with varying mixing times were recorded (400, 350, 300, 250, 200, 150, and 50 ms). From the resulting spectra, the integral ratio of the NOE peak to the inverted peak was plotted against the mixing time. ²⁵ The slope of this line was calculated using a linear fit. H-11 and H-26 were used as the calibration distance, setting it to 2.679 Å. As an internal check, the correlation between H-9 and H-25 was found to be 2.71 Å. This was in good agreement with the predicted value of 2.65 Å. Additionally, the distance measurement from H-6 to H-9 of 2.10 Å was in excellent agreement with the measurement from H-9 to H-6 of 2.09 Å.

Computational Details. Initial conformational analysis was performed in Spartan³⁹ using the MMFF molecular mechanics force field and random rotor conformational search with 100 conformers. Density functional theory calculations were performed using the Gaussian 09 package⁴⁰ or ORCA 4.0.1.⁴¹ ECD spectra were calculated by the TDDFT methodology at the ωB97XD/def2-TZVP level (UV shift of -1 nm and a σ value of 0.22 eV) utilizing CPCM in acetonitrile (compound 1), CAM-B3LYP/TZVP with IEFPCM in acetonitrile (UV shift of 6 nm and a σ value of 0.25 eV), or ωB97X-D3/def2-TZVP(-f) (UV shift of 20 nm and a σ value of 0.3 eV) utilizing CPCM in acetonitrile (compound 2). ECD spectra were simulated using SpecDis 1.71.⁴² High-accuracy ¹H NMR shifts were computed at the WP04/aug-cc-pVDZ level utilizing PCM in chloroform according to Wiitala et al.²³ For Stereofitter analysis, the original conformer populations, as well as newly generated conformers from the enantiomeric form 2R,3R,9R,11S, which were then reflected

back to 2S,3S,9S,11R, increasing the number of low-energy 2,3-anti conformers present in the 2S,3S,9S,11R conformer pool, were used. These conformer sets were subjected to QM geometry optimizations and frequency calculations at $M06-2X/6-31+G^*$. All 2,3-gauche conformers below 5 kcal and all 2,3-anti conformers for each possible configuration, 2S,3S,9R,11R, 2S,3S,9S,11R, 2S,3S,9R,11S, and 2S,3S,9S,11S, not exhibiting imaginary frequencies were analyzed with Stereofitter (Mestrelab)^{3a} utilizing NOE-derived distance and coupling constant constraints from Table 3. Single-point energies for all conformers found in the 2S,3S,9S,11R Stereofitter solutions were computed at the DLPNO-CCSD(T) level, ²⁴ with a def2-TZVP triple- ζ basis set using resolution of identity approximation for Coulomb integrals and COSX numerical integration for Hartree—Fock exchange, both with and without CPCM solvation (acetonitrile).

Antimicrobial Assays. Extracts and fractions were tested for inhibitory activity against *Staphylococcus aureus* (ATCC 25923), methicillin-resistant *Staphylococcus aureus* (ATCC BAA-41), multidrug-resistant *Staphylococcus aureus* (ATCC BAA-44), *Pseudomonas aeruginosa* (ATCC 15442), *Candida albicans* (ATCC 90027), *Candida krusei* (ATCC 34135), and *Mycobacterium smegmatis* (ATCC 14468) in microbroth assays performed following an established protocol. Fractions and pure compounds were tested at a concentration of 125 μ g/mL. All human pathogens used in the study were acquired from the American Type Culture Collection (ATCC, Manassas, VA, USA).

Cytotoxicity Assay. Cytotoxic activities of extracts and pure compounds were evaluated against colon (HCT-116) cancer models by measuring the reduction of the tetrazolium salt MTT (3-(4,5-dimethylthiazolyl-2)-2,5-diphenyltetrazolium bromide) by metabolically active cells following standard procedures.⁴⁴

Antioxidant Assay. Antioxidant activity was tested using the DPPH radical scavenging assay. Compounds were tested at 50 and 100 μ M in MeOH. DPPH final concentration was 0.05 mM. Vitamin C (25 μ M) was used as positive control. Absorbance at 517 nm was monitored every 10 min for 30 min, then every 30 min for 4 h. The percent of unreacted DPPH was quantified using a calibration curve at 517 nm.

Metal-Chelating Activity Assay. Fe chelating activity was tested with competition assays using FeCl₂ and ferrozine, ⁴⁶ which absorbs 562 nm light when complexed with ferrous ions. Test compounds were dissolved in DMSO and added to 96-well plates. Then, FeCl₂ in $\rm H_2O$ was added to the test compounds followed by the addition of ferrozine in $\rm H_2O$. After 10 min of incubation, the plates were read at 562 nm. Fungal metabolites were tested at 50 and 100 μ M. FeCl₂ and ferrozine were at a final concentration of 40 and 50 μ M, respectively. EDTA (50 μ M) was used as a positive control.

ASSOCIATED CONTENT

S Supporting Information

The Supporting Information is available free of charge on the ACS Publications website at DOI: 10.1021/acs.jnat-prod.9b00416.

NMR data for compounds 1, 2, 3a, and 3b; UV, ECD (experimental and theoretical spectra), and computational details for compound 1 and 2 (PDF)

AUTHOR INFORMATION

Corresponding Author

*E-mail: sandra.loesgen@oregonstate.edu, sandra.loesgen@whitney.ufl.edu.

ORCID ®

Torsten Bruhn: 0000-0002-9604-1004 Sandra Loesgen: 0000-0003-1090-564X

Present Address

§Whitney Laboratory for Marine Bioscience and Department of Chemistry, University of Florida, St. Augustine, Florida 32080, United States.

Notes

The authors declare no competing financial interest.

ACKNOWLEDGMENTS

This work was supported by OSU start-up funds and by the National Science Foundation under grant CHE 1808717. We wish to thank Bioviotica (Prof. Dr. A. Zeeck and H.-P. Kroll) for providing Aspergillus porosus. We also thank Drs. Oliver Schlörke and Jens Bitzer, who isolated the strain, and Barbara Schulz for initial strain identification. In addition, we thank Dr. L. Bermudez (Oregon State University) and Dr. M. Riscoe (Oregon Health and Science University) for antitubercular and antimalaria screening, respectively. We acknowledge the support of the Oregon State University's NMR Facility funded in part by the National Institutes of Health, HEI grant 1S10OD018518, and by the M. J. Murdock Charitable Trust grant no. 2014162. We thank Z. Zhu and Dr. B. Plitzko for performing the cytotoxicity assay, Prof. J. Stone (Oregon State University) for assistance with fungal taxonomy, and Profs. P. Proteau and J. Strother (Oregon State University) for fruitful discussions.

REFERENCES

- (1) (a) Chhetri, B. K.; Lavoie, S.; Sweeney-Jones, A. M.; Kubanek, J. *Nat. Prod. Rep.* **2018**, *35*, 514–531. (b) Chhetri, B. K.; Lavoie, S.; Sweeney-Jones, A. M.; Kubanek, J. *Nat. Prod. Rep.* **2018**, *35*, 1014–1015.
- (2) Newman, D. J.; Cragg, G. M. J. Nat. Prod. 2016, 79, 629–661. (3) (a) Navarro-Vázquez, A.; Gil, R. R.; Blinov, K. J. Nat. Prod. 2018, 81, 203–210. (b) Superchi, S.; Scafato, P.; Gorecki, M.; Pescitelli, G. Curr. Med. Chem. 2018, 25, 287–320. (c) Pescitelli, G.; Bruhn, T. Chirality 2016, 28, 466–474. (d) Grimblat, N.; Sarotti, A. M. Chem. Eur. J. 2016, 22, 12246–12261. (e) Lodewyk, M. W.; Siebert, M. R.; Tantillo, D. J. Chem. Rev. 2012, 112, 1839–1862.
- (4) Chen, A. J.; Hubka, V.; Frisvad, J. C.; Visagie, C. M.; Houbraken, J.; Meijer, M.; Varga, J.; Demirel, R.; Jurjević, Ž.; Kubátová, A.; Sklenář, F.; Zhou, Y. G.; Samson, R. A. Stud. Mycol. 2017, 88, 37–135
- (5) (a) Matsuzaki, K.; Tahara, H.; Inokoshi, J.; Tanaka, H. J. Antibiot. 1998, 51, 1004–1011. (b) Chiang, Y.-M.; Szewczyk, E.; Davidson, A. D.; Keller, N.; Oakley, B. R.; Wang, C. C. C. J. Am. Chem. Soc. 2009, 131, 2965–2970.
- (6) Stierle, D. B.; Stierle, A. A.; Ganser, B. K. J. Nat. Prod. 1999, 62, 1147–1150.
- (7) (a) Norte, M.; Cataldo, F.; González, A. G. *Tetrahedron Lett.* **1988**, 29, 2879–2880. (b) Calter, M. A.; Liao, W. *J. Am. Chem. Soc.* **2002**, 124, 13127–13129. (c) Cutignano, A.; Calado, G.; Gaspar, H.; Cimino, G.; Fontana, A. *Tetrahedron Lett.* **2011**, 52, 4595–4597.
- (8) Shen, W.; Mao, H.; Huang, Q.; Dong, J. Eur. J. Med. Chem. 2015, 97, 747-777.
- (9) Gao, J.-M.; Yang, S.-X.; Qin, J.-C. Chem. Rev. 2013, 113, 4755–4811.
- (10) Amico, V.; Cunsolo, F.; Piattelli, M.; Ruberto, G. Phytochemistry 1985, 24, 2663-2668.
- (11) Ellestad, G. A.; Kunstmann, M. P.; Mirando, P.; Morton, G. O. J. Am. Chem. Soc. 1972, 94, 6206–6208.
- (12) (a) Evidente, A.; Sparapano, L.; Motta, A.; Giordano, F.; Fierro, O.; Frisullo, S. *Phytochemistry* **1996**, 42, 1541–1546. (b) Sparapano, L.; Bruno, G.; Fierro, O.; Evidente, A. *Phytochemistry* **2004**, 65, 189–198.

(13) Lallemand, B.; Masi, M.; Maddau, L.; De Lorenzi, M.; Dam, R.; Cimmino, A.; Moreno y Banuls, L.; Andolfi, A.; Kiss, R.; Mathieu, V.; Evidente, A. *Phytochem. Lett.* **2012**, *5*, 770–775.

- (14) Mathieu, V.; Chantôme, A.; Lefranc, F.; Cimmino, A.; Miklos, W.; Paulitschke, V.; Mohr, T.; Maddau, L.; Kornienko, A.; Berger, W.; Vandier, C.; Evidente, A.; Delpire, E.; Kiss, R. Cell. Mol. Life Sci. 2015, 72, 3731–3746.
- (15) Yan, T.; Guo, Z. K.; Jiang, R.; Wei, W.; Wang, T.; Guo, Y.; Song, Y. C.; Jiao, R. H.; Tan, R. X.; Ge, H. M. *Planta Med.* **2013**, 79, 348–352.
- (16) White, T. J.; Bruns, T.; Lee, S.; Taylor, J. Amplification and direct sequencing of fungal ribosomal RNA genes for phylogenetics. In *PCR Protocols*; Innis, M. A.; Gelfand, D. H.; Sninsky, J. J.; White, T. J., Eds.; Academic Press: San Diego, 1990; pp 315–322.
- (17) Raja, H. A.; Miller, A. N.; Pearce, C. J.; Oberlies, N. H. J. Nat. Prod. 2017, 80, 756-770.
- (18) Glass, N. L.; Donaldson, G. C. Appl. Environ. Microbiol. 1995, 61, 1323-1330.
- (19) (a) Seco, J. M.; Quiñoá, E.; Riguera, R. Chem. Rev. **2004**, 104, 17–118. (b) Hoye, T. R.; Jeffrey, C. S.; Shao, F. Nat. Protoc. **2007**, 2, 2451.
- (20) Matsumori, N.; Kaneno, D.; Murata, M.; Nakamura, H.; Tachibana, K. J. Org. Chem. 1999, 64, 866–876.
- (21) (a) Kurz, M.; Schmieder, P.; Kessler, H. Angew. Chem., Int. Ed. Engl. 1991, 30, 1329–1331. (b) Uhrín, D.; Batta, G.; Hruby, V. J.; Barlow, P. N.; Kövér, K. E. J. Magn. Reson. 1998, 130, 155–161.
- (22) Willoughby, P. H.; Jansma, M. J.; Hoye, T. R. Nat. Protoc. 2014, 9, 643.
- (23) Wiitala, K. W.; Hoye, T. R.; Cramer, C. J. J. Chem. Theory Comput. 2006, 2, 1085–1092.
- (24) (a) Riplinger, C.; Neese, F. J. Chem. Phys. 2013, 138, 034106.
 (b) Riplinger, C.; Sandhoefer, B.; Hansen, A.; Neese, F. J. Chem. Phys. 2013, 139, 134101.
- (25) Hu, H.; Krishnamurthy, K. J. Magn. Reson. 2006, 182, 173-177.
- (26) Stott, K.; Keeler, J.; Van, Q. N.; Shaka, A. J. J. Magn. Reson. 1997, 125, 302-324.
- (27) Thrippleton, M. J.; Keeler, J. Angew. Chem., Int. Ed. 2003, 42, 3938–3941.
- (28) Kolmer, A.; Edwards, L. J.; Kuprov, I.; Thiele, C. M. J. Magn. Reson. 2015, 261, 101–109.
- (29) (a) Baell, J. B.; Holloway, G. A. J. Med. Chem. **2010**, 53, 2719–2740. (b) Baell, J. B. J. Nat. Prod. **2016**, 79, 616–628.
- (30) Smilkstein, M.; Sriwilaijaroen, N.; Kelly, J. X.; Wilairat, P.; Riscoe, M. Antimicrob. Agents Chemother. 2004, 48, 1803–1806.
- (31) (a) Bermudez, L. E.; Meek, L. Tuberc. Res. Treat. **2014**, 2014, 530814–530815. (b) Bermudez, L. E.; Kolonoski, P.; Wu, M.; Aralar, P. A.; Inderlied, C. B.; Young, L. S. Antimicrob. Agents Chemother. **1999**, 43, 1870–1874.
- (32) Adpressa, D. A.; Loesgen, S. Chem. Biodiversity 2016, 13, 253-259.
- (33) Tamura, K. Mol. Biol. Evol. 1992, 9, 678-87.
- (34) Kimura, M. J. Mol. Evol. 1980, 16, 111-20.
- (35) Clark, K.; Karsch-Mizrachi, I.; Lipman, D. J.; Ostell, J.; Sayers, E. W. Nucleic Acids Res. 2016, 44, D67–D72.
- (36) Altschul, S. F.; Gish, W.; Miller, W.; Myers, E. W.; Lipman, D. J. J. Mol. Biol. 1990, 215, 403–10.
- (37) Kumar, S.; Stecher, G.; Tamura, K. Mol. Biol. Evol. 2016, 33,
- (38) UV absorbance spectra of 3a and 3b from LCMS analysis. No concentration available.
- (39) Hanwell, M. D.; Curtis, D. E.; Lonie, D. C.; Vandermeersch, T.; Zurek, E.; Hutchison, G. R. J. Cheminf. 2012, 4, 1–17.
- (40) Frisch, M. J.; Trucks, G. W.; Schlegel, H. B.; Scuseria, G. E.; Robb, M. A.; Cheeseman, J. R.; Scalmani, G.; Barone, V.; Mennucci, B.; Petersson, G. A.; Nakatsuji, H.; Caricato, M.; Li, X.; Hratchian, H. P.; Izmaylov, A. F.; Bloino, J.; Zheng, G.; Sonnenberg, J. L.; Hada, M.; Ehara, M.; Toyota, K.; Fukuda, R.; Hasegawa, J.; Ishida, M.; Nakajima, T.; Honda, Y.; Kitao, O.; Nakai, H.; Vreven, T.; Montgomery, J. A., Jr.; Peralta, J. E.; Ogliaro, F.; Bearpark, M. J.;

- Heyd, J.; Brothers, E. N.; Kudin, K. N.; Staroverov, V. N.; Kobayashi, R.; Normand, J.; Raghavachari, K.; Rendell, A. P.; Burant, J. C.; Iyengar, S. S.; Tomasi, J.; Cossi, M.; Rega, N.; Millam, N. J.; Klene, M.; Knox, J. E.; Cross, J. B.; Bakken, V.; Adamo, C.; Jaramillo, J.; Gomperts, R.; Stratmann, R. E.; Yazyev, O.; Austin, A. J.; Cammi, R.; Pomelli, C.; Ochterski, J. W.; Martin, R. L.; Morokuma, K.; Zakrzewski, V. G.; Voth, G. A.; Salvador, P.; Dannenberg, J. J.; Dapprich, S.; Daniels, A. D.; Farkas, Ö.; Foresman, J. B.; Ortiz, J. V.; Cioslowski, J.; Fox, D. J. *Gaussian 09*; Gaussian, Inc.: Wallingford, CT, USA, 2009.
- (41) Neese, F. Wiley Interdiscip. Rev. Comput. Mol. Sci. 2018, 8, No. e1327.
- (42) Bruhn, T.; Schaumloffel, A.; Hemberger, Y.; Bringmann, G. Chirality 2013, 25, 243–9.
- (43) L, N. C. f. C. Approved Standard M02-A11 and M100-S25. NCCLS: Wayne, PA, USA, 2002.
- (44) Riss, T. L., Moravec, R. A., Niles, A. L., Duellman, S., Benink, H. A., Worzella, T. J., Minor, L. Cell Viability Assays. In *Assay Guidance Manual*; Sittampalam, G. S.; Coussens, N. P.; Nelson, H. E. A., Eds.; Eli Lilly & Company, and the National Center for Advancing Translational Sciences (NIH): Bethesda, MD, 2013.
- (45) (a) Brand-Williams, W.; Cuvelier, M. E.; Berset, C. LWT-Food Sci. Technol. 1995, 28, 25–30. (b) Sharma, O. P.; Bhat, T. K. Food Chem. 2009, 113, 1202–1205.
- (46) Stookey, L. L. Anal. Chem. 1970, 42, 779-781.